Origin of SAXS intensity in the low-q region during the early stage of polymer crystallization from both the melt and glassy state

Takashi Konishi,[1,*] Daisuke Okamoto,[1] Daisuke Tadokoro,[1] Yoshitaka Kawahara,[1] Koji Fukao,[2] and Yoshihisa Miyamoto[1]

[1]*Graduate School of Human and Environmental Studies, Kyoto University, Kyoto 606-8501, Japan*

[2]*Department of Physics, Ritsumeikan University, Noji-Higashi 1-1-1, Kusatsu 525-8577, Japan*

(Received 29 December 2017; published 2 October 2018)

The isothermal crystallization from the melt and glassy state of poly(trimethylene terephthalate) has been studied with wide-angle x-ray diffraction, small-angle x-ray scattering (SAXS), and ultrasmall-angle x-ray scattering (USAXS). Large scattering intensity in the low-q region has been observed with SAXS and USAXS during the early stage of melt and glass crystallizations. We have quantitatively analyzed the x-ray results using the scattering equations which can simultaneously deal with the hierarchical structures consisting of the crystallites and their aggregates. The results reveal the crystallization mechanism in which the crystalline nodules cover the entire sample with the aggregation regions. The conclusion quantitatively shows that the large SAXS intensity is not due to the density fluctuations of the liquid state but due to the correlations among the heterogeneous aggregation regions of the nodules.

DOI: 10.1103/PhysRevMaterials.2.105602

I. INTRODUCTION

Most materials crystallize when quenched from the melting temperature or annealed above the glass transition temperature. Despite the importance of crystallization in many fields, a complete understanding of the crystallization process is one of the most difficult problems remaining in condensed matter physics. Traditionally, the classical nucleation theory has explained the crystal nucleation and growth mechanism; however, recently the existence of density fluctuations with the formation of precursor domains during the initial stage of crystallization has been discussed using experimental [1–6], simulation [7,8], and theoretical studies [9,10].

There is a long-standing controversy regarding the existence of density fluctuations during the early stage of polymer crystallization [11–27]. Some groups have reported that the fluctuations obtained with small-angle x-ray scattering (SAXS) undergo a spinodal liquid-liquid phase separation due to orientational fluctuations of stiff segments [13–15]. The experimental results have been supported by theoretical [19] and simulation studies [24]. On the other hand, Muthukumar and coworkers have reported that the fluctuations originate from precursors obtained in simulations [20–23] and theoretical studies [22]. The experimental evidence of the precursors has been reported [11,16,25–27]. The origin of the fluctuations has, however, not been understood sufficiently since the intensity of the fluctuations in the experimental results is very weak [28]. Understanding the density fluctuations will become key in solving polymer crystallization.

Recently, Chuang and coworkers [29,30] have reported that a large SAXS intensity in the low-q region during the induction period of crystallization for poly(trimethylene terephthalate) (PTT) from the glassy state and that the SAXS intensity comes from the formation of the mesomorphic domains. The purpose of this paper is to elucidate the origin of these SAXS intensities during the early stage of polymer crystallization. In order to achieve this purpose, we have investigated the crystallization processes from the melt state and the glassy state using x-ray techniques. We have analyzed the experimental results using scattering equations which can simultaneously deal with the hierarchical structures consisting of the crystallites and their aggregates.

II. EXPERIMENT

The polymer sample used in this study was PTT. The melting and the glass transition temperatures were determined as 233 and 45 °C, respectively, by differential scanning calorimetry. The PTT films were isothermally crystallized at crystallization temperatures T_c, between 50 and 70 °C, from the melt state and the glassy state. The glass sample was prepared by melting at 280 °C for 1 min and quenching the molten PTT film of about 150 μm thickness into ice water at 0 °C.

The isothermal crystallization processes were investigated by simultaneous small-angle x-ray scattering and wide-angle x-ray diffraction (SAXS/WAXD) and ultrasmall-angle x-ray scattering (USAXS). The camera lengths for WAXD, SAXS, and USAXS were 100, 1500, and 4000 mm, respectively. The wavelengths λ for WAXD/SAXS and USAXS were 0.9 and 1.2 Å, respectively. The measurements were performed using the beam line BL-40B2 at SPring-8, Nishiharima, Japan. USAXS, SAXS, and WAXD cover the ranges of scattering vector $q = 4\pi \sin\theta/\lambda$ from 0.002 to 0.03, 0.02 to 0.2, and 0.5 to 3.0 Å^{-1}, respectively, where 2θ is the scattering angle. The temperature of the samples was controlled using a Linkam LK300 and THMS600.

III. RESULTS AND DISCUSSION

Figure 1(a) shows the WAXD profiles as a function of crystallization time t_c for PTT isothermally crystallized at

*konishi.takashi.8c@kyoto-u.ac.jp

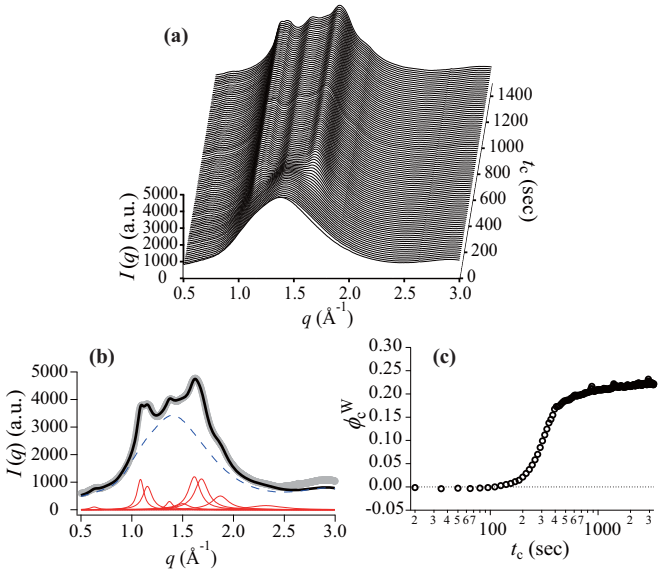

FIG. 1. (a) WAXD profiles and (c) crystallinity ϕ_c^W as a function of t_c for PTT crystallized at 60 °C from the melt. (b) The WAXD profile of PTT crystallized at 60 °C for 1000 sec from the melt state. The gray circles in (b) show the experimentally observed intensity. The thick solid black curve is the sum of the crystalline components (thin solid line) and the amorphous component (broken line). ϕ_c^W in (c) is calculated from the WAXD profiles in (a).

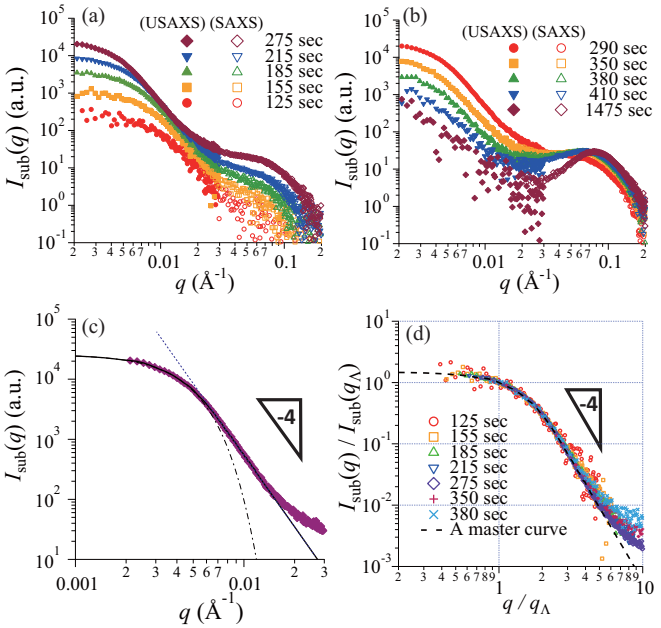

FIG. 2. SAXS and USAXS profiles $I_{sub}(q)$ as a function of t_c for PTT crystallized at 60 °C from the melt state (a) until and (b) after 280 sec, (c) the USAXS profile of PTT crystallized for 275 sec, and (d) the USAXS profiles normalized by q_Λ and $I_{sub}(q_\Lambda)$ in (a) and (b). The solid curves in (c) are the fitting curve using $a\exp(-b^2q^2)$ (chain curve) and cq^{-4} (dotted curve). The broken curve in (d) is a master curve. The right triangles in (c) and (d) indicate a slope of −4.

60 °C from the melt state. The WAXD profiles show the amorphous scattering just after quenching to 60 °C. Figure 1(b) shows the WAXD profile of PTT crystallized for $t_c = 1000$ sec. The Bragg peaks at $q = 0.63$, 1.09, 1.15, 1.37, 1.50, 1.62, 1.69, 1.87, and 2.32 Å^{-1} can be separated from the WAXD profile by using a Lorentzian function and indicate the triclinic crystalline structure of PTT [37]. The observed WAXD intensity can be expressed by the sum of amorphous and crystalline components: the WAXD result does not show any mesomorphic component [29] during crystallization. The crystallinity ϕ_c from the WAXD result, ϕ_c^W, was estimated to be 22% from the ratio in integrated intensity between the amorphous halo and the Bragg peaks. Figure 1(c) shows the t_c-dependent ϕ_c^W of the melt-crystallized sample.

Figures 2(a) and 2(b) show the t_c-dependent SAXS and USAXS profiles $I_{sub}(q)$ for PTT isothermally crystallized at 60 °C from the melt state until and after 280 sec, respectively. For the USAXS and SAXS measurements, the intensity $I(q, t_c = 0)$ is subtracted from $I(q, t_c)$, $I_{sub}(q) = I(q, t_c) - I(q, t_c = 0)$. Since $I_{sub}(q)$ shows different behaviors in the low- and high-q regions, $I_{sub}(q)$ can be given by $I_{sub}(q) = I_L(q) + I_H(q)$, where $I_L(q)$ and $I_H(q)$ mainly represent $I_{sub}(q)$ at $q < 0.02$ Å^{-1} and $q > 0.02$ Å^{-1}, respectively. The intensity $I_L(q)$ decreases with q, and increases with t_c until 280 sec and then decreases after 280 sec. On the other hand, $I_H(q)$ has a peak around $q = 0.08$ Å^{-1}, and monotonically increases with t_c. The features shown in the SAXS intensity correspond well with those obtained by Chuang and coworkers [29]. Electron micrographs for PTT crystallized at 55 °C from the glassy state do not show any spherulites at the micrometer scale but show a crystalline nodular morphology at the nanometer scale separated by an amorphous region [29]. Such nodule structure has been observed for other polymers [31–36]. The peak of $I_H(q)$ corresponds to quasiperiodic correlations among the nodules [29,30].

The t_c-dependent invariant Q, defined by $Q = \int_0^\infty q^2 I(q) dq$, will be discussed here. The invariant for $I_{sub}(q)$, Q_T, is also divided into two components: Q for $I_L(q)$ in the q range from $q = 0.002$–0.02 Å^{-1}, Q_L, and Q for $I_H(q)$ from 0.02 to 0.2 Å^{-1}, Q_H. The dependencies of invariants Q_T, Q_L, and Q_H on t_c are shown in Fig. 3(a). The values of Q_T and Q_H monotonically increase with time, while Q_L increases until 280 sec and decreases after 280 sec. The value of Q_L becomes zero when Q_T and Q_H reach their saturations at about 400 sec. The value of $Q_T(t_c = 280$ sec) is about half of $Q_T(t_c = 400$ sec).

The value of Q_T is proportional to $\phi_c(1 - \phi_c)$ since there are only two components, amorphous and crystalline, during crystallization in the WAXD profiles (Fig. 1). t_c-dependent Q_T is similar to t_c-dependent ϕ_c^W in Figs. 1(c) and 3(b) since $\phi_c < 0.5$. Q_H [$I_H(q)$] and Q_L [$I_L(q)$] originate from the correlations among structures on spatial scales of roughly 100 and 1000 Å, respectively. The monotonic increase in Q_H shows an increase in the nodular aggregates with t_c. The distribution of the aggregates at 1000 Å scale is not quasiperiodic but random since $I_L(q)$ monotonically decreases with q (Fig. 2). t_c-dependent Q_L increases from zero, reaches a maximum, and decreases to zero. This behavior shows that the nodular aggregates randomly grow in the homogeneous supercooled liquid and eventually cover the entire sample.

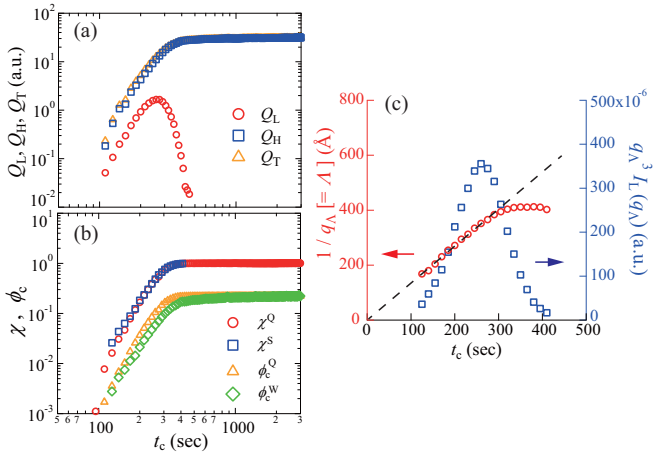

FIG. 3. t_c-dependent (a) Q_T, Q_H, and Q_L, (b) χ and ϕ_c obtained from SAXS and WAXD results, and (c) $1/q_\Lambda$ and $q_\Lambda^3 I(q_\Lambda)$. In (b) the values of χ^Q and χ^S were obtained from Q_H (open circles) and from $q_\Lambda^3 I(q_\Lambda)$ (open squares), respectively. The values of ϕ_c were obtained from the Q values (open triangles) and from the WAXD results (open diamonds) in Fig. 1(c), respectively.

Thus, $I_L(q)$ originates from correlations among the randomly distributed regions of the aggregated nodules, and $I_H(q)$ originates from correlations among the nodules in the regions. The results in Fig. 3(a), therefore, show the process that the crystalline nodules cover the entire PTT sample with the aggregation regions.

The crystallization mechanism with the hierarchical structures consisting of the nodules and their aggregates is expressed using the following equations. We consider the situation when the crystallization is completed; that is, the N crystalline nodules cover the entire sample with volume V. The position of the ith nodule is expressed as $\boldsymbol{r_i} + \boldsymbol{R_i}$, where $\boldsymbol{r_i}$ is the center of mass for the ith nodule, and $\boldsymbol{R_i}$ is the position from the center of mass for the ith nodule. Assuming all the nodules have the same shape, we define the density distribution function for the nodular shape as $\rho_p(\boldsymbol{R_i})$, which indicates 1 inside the ith nodule and 0 outside that. The density distribution function of the nodules covering the entire sample, $\rho_n(\boldsymbol{r})$, is written as $\rho_n(\boldsymbol{r}) = \rho_a + (\Delta\rho_{ac}) \sum_i^N \delta(\boldsymbol{r} - \boldsymbol{r_i}) * \rho_p(\boldsymbol{r})$, where $*$ indicates convolution, ρ_a and ρ_c indicate the densities of the amorphous and crystalline components, respectively, and $\Delta\rho_{ac} = \rho_c - \rho_a$. The one-dimensional $\rho_n(\boldsymbol{r})$ is illustrated in Fig. S1(a) of the Supplemental Material [38]. The volume fraction of the packed nodules in the sample is represented by $\psi = Nv/V$ where v is the volume of each nodule.

In order to describe the formation process of the nodule aggregation, we introduce the distribution function of the region of the aggregated nodules, $\eta(\boldsymbol{r})$, which indicates 1 inside the region and 0 outside that [Fig. S1(b)]. Thus, the position of the nodules in the aggregation regions during the crystallization is given by $\eta(\boldsymbol{r})\rho_s(\boldsymbol{r})$, where $\rho_s(\boldsymbol{r}) = \sum_i^N \delta(\boldsymbol{r} - \boldsymbol{r_i})$. The volume fraction of the aggregation regions is represented by χ. The total distribution function $\rho_{\rm tot}(\boldsymbol{r})$ can be described as $\rho_{\rm tot}(\boldsymbol{r}) = \rho_a + (\Delta\rho_{ac})\{\eta(\boldsymbol{r})\rho_s(\boldsymbol{r})\} * \rho_p(\boldsymbol{r})$ [Fig. S1(c)]. The volume fraction of the nodules in the system corresponds to the crystallinity $\phi_c = \chi\psi$.

The one-dimensional scattering intensity in the isotropic system, $I_{\rm tot}(q)$, can be given by $I_{\rm tot}(q) = (1/V)\langle \int \rho_{\rm tot}(\boldsymbol{r'})\rho_{\rm tot}(\boldsymbol{r} + \boldsymbol{r'}) e^{-i\boldsymbol{q}\cdot\boldsymbol{r}} d\boldsymbol{r'} d\boldsymbol{r} \rangle$, where the operator $\langle \cdots \rangle$ denotes the ensemble and orientational averages:

$$\begin{aligned} I_{\rm tot}(q) = (\Delta\rho_{ac})^2 \{ & \chi(1-\chi)\psi^2 S_\eta(q) \\ & + \psi(1-\psi)\chi^2 S_n(q) \\ & + \chi(1-\chi)\psi(1-\psi) S_{\eta(q)} * S_n(q) \} P_n(q), \end{aligned} \tag{1}$$

where $S_\eta(q)$, $S_n(q)$, and $P_n(q)$ are the ensemble- and orientational-averaged Fourier transforms of normalized correlation functions of the distribution functions for $\eta(\boldsymbol{r})$, $\rho_s(\boldsymbol{r})$, and $\rho_p(\boldsymbol{r})$, respectively.

Assuming the size of the aggregation region is sufficiently larger than the nodular size, $S_\eta(q)$ can be regarded as the delta function for $S_n(q)$, and $P_n(q)$ can be regarded as unity for $S_\eta(q)$. Thus Eq. (1) can be rewritten as

$$\begin{aligned} I_{\rm tot}(q) = (\Delta\rho_{ac})^2 \{ & \chi(1-\chi)\psi^2 S_\eta(q) \\ & + \chi\psi(1-\psi) S_n(q) P_n(q) \}. \end{aligned} \tag{2}$$

Equation (2) represents the intensity $I_{\rm sub}(q)$ obtained from the SAXS results. The first and second terms on the right-hand side of Eq. (2) should be regarded as $I_L(q)$ and $I_H(q)$, respectively, and give

$$Q_T = 2\pi^2 (\Delta\rho_{ac})^2 \phi_c (1 - \phi_c), \tag{3}$$

$$Q_L = 2\pi^2 (\Delta\rho_{ac})^2 \chi(1-\chi)\psi^2, \tag{4}$$

$$Q_H = 2\pi^2 (\Delta\rho_{ac})^2 \chi\psi(1-\psi). \tag{5}$$

These equations satisfy $Q_T = Q_L + Q_H$. The detailed derivation of Eqs. (1)–(5) is described in Sec. 1 of the Supplemental Material [38]. The value of χ is between 0 and 1 and ψ is considered to be constant during crystallization. Thus, Q_T and Q_H monotonically increase while Q_L increases and then decreases with time. Assuming ψ is constant, the values of χ, χ^Q, ψ, ψ^Q, and ϕ_c, ϕ_c^Q can be calculated from Q depicted in Fig. 3(a) using Eqs. (3)–(5). The calculated result leads to $\psi^Q = 0.22$ and t_c-dependent χ^Q and ϕ_c^Q are shown in Fig. 3(b). The behavior of χ^Q is similar to those of ϕ_c^W and Q_T. The comparison shows that Eq. (2) quantitatively represents $I_{\rm sub}(q)$. The above discussion demonstrates that the density fluctuations, which give rise to $I_L(q)$, do not come from the fluctuations in the supercooled liquid with orientational order [13–15,19,29], but do come from the correlations among the heterogeneous aggregation regions of nodules. Although the time evolutions of $\rho_s(\boldsymbol{r})$ and $\rho_p(\boldsymbol{r})$ have been ignored in this analysis, the scattering equation can explain the obtained experimental results well. The time evolutions of $\rho_s(\boldsymbol{r})$ and $\rho_p(\boldsymbol{r})$ have been reported in detail by Chuang and coworkers [29].

In order to estimate the size and shape of the aggregates, we analyze t_c-dependent $I_L(q)$ using the characteristic wave length, q_Λ, which is defined as the first moment of $I_L(q)$, $q_\Lambda = \int_0^\infty q I_L(q) dq / \int_0^\infty I_L(q) dq$. For the numerical estimation of q_Λ, $I_L(q)$ is extrapolated by $a \exp(-b^2 q^2)$ in the low-q

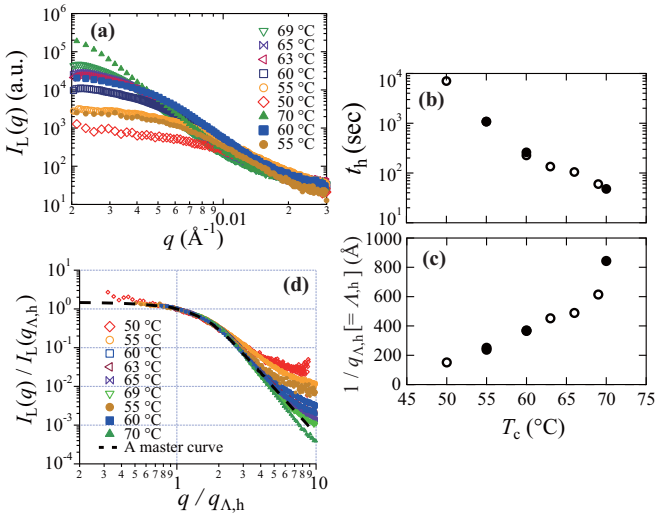

FIG. 4. (a) $I_L(q)$ for PTT crystallized at T_c for t_h from the melt state (filled symbols), and the glassy state (open ones), T_c-dependent (b) t_h and (c) $1/q_{\Lambda,h}$, and (d) $I_L(q)$ normalized by $q_{\Lambda,h}$ and $I_L(q_{\Lambda,h}, t_h)$ in (a).

region and cq^{-4} in the high-q region where a, b, and c are constants [Fig. 2(c)]. Figure 2(d) shows $I_L(q)$ normalized by q_Λ and $I_{\rm sub}(q_\Lambda)$. Normalized $I_L(q)$ shows that $I_L(q)$ can be scaled.

Figure 3(c) shows t_c-dependent $1/q_\Lambda$ and $q_\Lambda^3 I_L(q_\Lambda)$. $1/q_\Lambda$ can be regarded as a characteristic length, Λ, of the aggregation region. Λ linearly increases with t_c and becomes constant at $t_c > 300$ sec. $q_\Lambda^3 I_L(q_\Lambda)$ is proportional to $\chi(1-\chi)\psi^2$ since the scalable structure factor in the three-dimensional two-component system is proportional to $q_\Lambda^{-3} F(q/q_\Lambda)$ [Eq. (S4)], where $F(x)$ is a time-independent scaling function [39–42]. The detailed derivation of these relations is described in Sec. 2 of the Supplemental Material [38]. The value of $\chi(1-\chi)\psi^2$ has a maximum at $t_c = 275$ sec. The t_c-dependent χ and χ^S can be obtained in Fig. 3(b) because of constant ψ and it also corresponds to χ^Q. t_c-dependent ϕ_c^Q obtained from the SAXS results quantitatively agrees with t_c-dependent ϕ_c^W from the WAXD results. The kinetics of the nodular aggregates is different from the spinodal-like kinetics [15,19].

To further investigate the nature of the nodular aggregations, x-ray measurements of melt- and glass-crystallized PTT for different T_c have been performed. The increase and then decrease in $I_L(q)$ with time can be observed for both melt and glass crystallization. The time t_h at which $I_L(q)$ becomes maximum yields $\chi = 0.5$. Figure 4(a) shows $I_L(q)$ for PTT crystallized at T_c for t_h from the melt state and the glassy state. T_c-dependent t_h is shown in Fig. 4(b). The increase in t_h with decreasing T_c in Fig. 4(c) is due to the increase in structural relaxation time close to the glass transition temperature. q_Λ estimated from $I_L(q, t_c = t_h)$ in Fig. 4(a) is denoted as $q_{\Lambda,h}$, and $1/q_{\Lambda,h}$ as Λ_h. T_c-dependent $1/q_{\Lambda,h}$ are shown in Fig. 4(c). Figure 4(c) shows that Λ_h increases with increasing T_c. Figure 4(d) shows $I_L(q, t_h)$ normalized by $q_{\Lambda,h}$ and $I_L(q_{\Lambda,h})$. Normalized $I_L(q, t_h)$ shows that all $I_L(q, t_h)$ can be scaled considering the deviation in the high-q regions by $I_H(q)$. The above results show that t_h and Λ_h depend only on T_c regardless of the initial melt or glassy state.

The experimental results reveal the following: (1) The scattering intensity in the low-q region $I_L(q)$ has been observed during the early stage of the melt and glass crystallization. (2) $I_L(q)$ originates from the correlations among the aggregation regions of the crystalline nodules. (3) The t_c dependence of ϕ_c obtained from the SAXS result quantitatively agrees with that from the WAXD result. (4) The nodular aggregation regions spread with linearly increasing Λ during the early stage and eventually cover the entire sample. (5) $I_L(q)$ observed for all conditions can be scaled. Panine and coworkers [25] have reported the simultaneous observation of the SAXS and WAXD signals and the time evolution of each signal during the early stage of crystallization of isotactic polypropylene (iPP). As mentioned above, this paper reveals the crystallization process with the nodular aggregation, especially the quantitative agreement between the SAXS and WAXD results and the nature of the aggregation regions. Meanwhile, the origin of the aggregation mechanism of nodules remains unclear.

The results in the present study show that the nodules might easily form around the already formed nodular aggregates. Muthukumar's model explains the early stage of nucleation by precursor "baby nuclei" followed by a cooperative coarsening of these multiple nuclei on the basis of the entropic effect of the polymer chain between baby nuclei. Miyoshi and coworkers [27] have reported using NMR techniques that there are chain foldings even in the nodules of iPP and that the NMR results are direct evidence of the cooperative coarsening of the nodules. Although direct evidence of the precursors is absent from our experimental results, we suggest that the possible origin of the nodular aggregates is the formation of precursors before crystallization. More specifically, the precursor regions, where crystallization easily occurs, form first followed by a number of crystalline nodules forming in each precursor region. The nodular aggregates might come from the entropic effect of the precursor. This crystallization process, with formation of precursors, has been reported in other systems [1–10]. The origin of the nodular aggregates should be investigated carefully in the future.

IV. SUMMARY

In summary, the crystallization of PTT from the melt and glassy state has been investigated with x-ray techniques. The SAXS intensity in the low-q region has been observed during the early stage of not only the glass crystallization but also the melt crystallization. The SAXS intensity observed in the present study is not due to the density fluctuations of the liquid state but due to the heterogeneous aggregations of nodules. The regions of the aggregated nodules linearly increase with time and eventually cover the entire sample. The proposed crystallization mechanism can quantitatively explain the experimental results using the scattering equations which can simultaneously deal with the hierarchical structures. The origin of nodular aggregation still remains an open question and could be key in solving polymer crystallization.

ACKNOWLEDGMENTS

This work was partially supported by JSPS KAKENHI Grant No. JP25800236, and the Kyoto University Foundation. The x-ray experiments were performed at the BL-40B2 of SPring-8 with the approval of the Japan Synchrotron Radiation Research Institute (JASRI) (Proposals No. 2015B1192, No. 2016A1340, and No. 2017A1497).

[1] K. Schätzel and B. J. Ackerson, Phys. Rev. E **48**, 3766 (1993).
[2] P. R. T. Wolde and D. Frenkel, Science **277**, 1975 (1997).
[3] U. Gasser, E. R. Weeks, A. Schofield, P. N. Pusey, and D. A. Weitz, Science **292**, 258 (2001).
[4] H. J. Schöpe, G. Bryant, and W. van Megen, Phys. Rev. Lett. **96**, 175701 (2006).
[5] J. R. Savage and A. D. Dinsmore, Phys. Rev. Lett. **102**, 198302 (2009).
[6] A. Sanz, A. Nogales, I. Puente-Orench, M. Jimenez-Ruiz, and T. A. Ezquerra, Phys. Rev. Lett. **107**, 025502 (2011).
[7] T. Schilling, H. J. Schöpe, M. Oettel, G. Opletal, and I. Snook, Phys. Rev. Lett. **105**, 025701 (2010).
[8] J. Russo and H. Tanaka, Sci. Rep. **2**, 505 (2012).
[9] J. F. Lutsko and G. Nicolis, Phys. Rev. Lett. **96**, 046102 (2006).
[10] J. F. Lutsko, J. Chem. Phys. **136**, 034509 (2012).
[11] K. Fukao and Y. Miyamoto, Phys. Rev. Lett. **79**, 4613 (1997).
[12] M. Soccio, A. Nogales, N. Lotti, A. Munari, and T. A. Ezquerra, Phys. Rev. Lett. **98**, 037801 (2007).
[13] M. Imai, K. Mori, T. Mizukami, K. Kaji, and T. Kanaya, Polymer **33**, 4451 (1992).
[14] N. J. Terrill, P. A. Fairclough, E. Towns-Andrews, B. U. Koanschek, R. J. Young, and A. J. Ryan, Polymer **39**, 2381 (1998).
[15] K. Kaji, K. Nishida, T. Kanaya, G. Matsuba, T. Konishi, and M. Imai, Adv. Polym. Sci. **191**, 187 (2005).
[16] T. A. Ezquerra, E. López-Cabarcos, B. S. Hsiao, and F. J. Baltà-Calleja, Phys. Rev. E **54**, 989 (1996).
[17] Y. Akpalu, L. Kielhorn, B. S. Hsiao, R. S. Stein, T. P. Russell, J. van Egmond, and M. Muthukumar, Macromolecules **32**, 765 (1999).
[18] S. Sasaki, K. Tashiro, M. Kobayashi, Y. Izumi, and K. Kobayashi, Polymer **40**, 7125 (1999).
[19] P. D. Olmsted, W. C. K. Poon, T. C. B. McLeish, N. J. Terrill, and A. J. Ryan, Phys. Rev. Lett. **81**, 373 (1998).
[20] C. Liu and M. Muthukumar, J. Chem. Phys. **101**, 5343 (1994).
[21] P. Welch and M. Muthukumar, Phys. Rev. Lett. **87**, 218302 (2001).
[22] M. Muthukumar, Philos. Trans. R. Soc. London A **361**, 539 (2003).
[23] P. M. Welch, J. Chem. Phys. **146**, 044901 (2017).
[24] R. H. Gee, N. M. Lacevic, and L. E. Fried, Nat. Mater. **5**, 39 (2006).
[25] P. Panine, E. Di Cola, M. Sztucki, and T. Narayanan, Polymer **49**, 676 (2008).
[26] Y. L. Hong, S. Yuan, Z. Li, Y. Ke, K. Nozaki, and T. Miyoshi, Phys. Rev. Lett. **115**, 168301 (2015).
[27] S. Yuan, Z. Li, Y. Hong, Y. Ke, J. Kang, A. Kamimura, A. Otsubo, and T. Miyoshi, ACS Macro Lett. **4**, 1382 (2015).
[28] Z. G. Wang, B. S. Hsiao, E. B. Sirota, P. Agarwal, and S. Srinivas, Macromolecules **33**, 978 (2000).
[29] W. T. Chuang, W. B. Su, U. S. Jeng, P. D. Hong, C. J. Su, C. H. Su, Y. C. Huang, K. F. Laio, and A. C. Su, Macromolecules **44**, 1140 (2011).
[30] J. B. Jheng, W. T. Chuang, P. D. Hong, Y. C. Huang, U. S. Jeng, C. J. Su, and G. R. Pan, Polymer **54**, 6242 (2013).
[31] J. J. Klement and P. H. Geil, J. Macromol. Sci., Part B: Phys. **5**, 505 (1971); **5**, 535 (1971).
[32] T. Ogawa, H. Miyaji, and K. Asai, J. Phys. Soc. Jpn. **54**, 3668 (1985).
[33] C. C. Hsu, P. H. Geil, H. Miyaji, and K. Asai, J. Polym. Sci., Part B: Polym. Phys. **24**, 2379 (1986).
[34] D. T. Grubb and D. Y. Yoon, Polym. Commun. (Guildford, England) **27**, 84 (1986).
[35] C. H. Su, U. Jeng, S. H. Chen, S. J. Lin, Y. T. Ou, W. T. Chuang, and A. C. Su, Macromolecules **41**, 7630 (2008).
[36] T. Konishi and Y. Miyamoto, Macromolecules **43**, 375 (2010).
[37] S. Poulin-Dandurand, S. Pérez, J. Revol, and F. Brisse, Polymer **20**, 419 (1979).
[38] See Supplemental Material at http://link.aps.org/supplemental/10.1103/PhysRevMaterials.2.105602 for an image of the one-dimensional density distribution functions, the derivation of the scattering intensity equations, and the scaling procedure using the scattering theory.
[39] H. Furukawa, Phys. Rev. Lett. **43**, 136 (1979).
[40] H. Furukawa, Phys. Rev. A **23**, 1535 (1981).
[41] M. Carpineti and M. Giglio, Phys. Rev. Lett. **68**, 3327 (1992).
[42] J. Bibette, T. G. Mason, Hu Gang, and D. A. Weitz, Phys. Rev. Lett. **69**, 981 (1992).